Energy 281 (2023) 128243

Contents lists available at ScienceDirect

Energy

journal homepage: www.elsevier.com/locate/energy

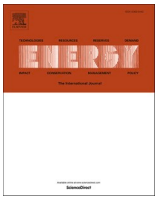

Study of the effects of thermally thin and thermally thick particle approaches on the Eulerian modeling of a biomass combustor operating with wood chips

M.A. Gómez [a,*], C. Álvarez-Bermúdez [a], S. Chapela [a], A. Anca-Couce [b,c], J. Porteiro [a]

[a] CINTECX, Grupo de Tecnología Energética (GTE), Universidade de Vigo, Lagoas-Marcosende s/n, 36310, Vigo, Spain
[b] Graz University of Technology, Institute of Thermal Engineering, Inffeldgasse 25/B, 8010, Graz, Austria
[c] Carlos III University of Madrid, Thermal and Fluids Engineering Department, Avda. de La Universidad 30, 28911, Leganés, Madrid, Spain

ARTICLE INFO

Keywords:
Biomass
Combustion
Eulerian
Thermally thin
Thermally thick

ABSTRACT

Two particle treatments, thermally thin and thick, are applied to Eulerian combustion modeling for biomass packed beds and tested through the simulation of an experimental plant. The paper shows the efficiency of the Eulerian approach for large packed beds and tests the behavior of both particle treatments, tested with in-bed and flame temperatures and released volatiles measurements at different locations, which is not common in the literature for a full size boiler.

Both approaches are implemented in a model with a comprehensive framework that includes several sub-models for the thermal conversion kinetics, bed motion, heat and mass transfer with the gas phase, and gas flow and reaction. Two experiments are performed with wood chips fuels with different moisture contents. The simulations of the two cases result in reasonably good predictions for both particle treatments. The results are similar for higher moisture content and, for the low-moisture test, the bed temperature distribution and reaction fronts are slightly different due to the different predictions of the drying and devolatilization fronts. The volatile measurements show that the T. Thin model results in slightly more accurate predictions than the T. Thick, possibly because the wood chips have a more thermally thin behavior.

1. Introduction

Multiple approaches have been used in recent decades to address the challenge of simulating the combustion process of a biomass packed bed through Computational Fluid Dynamics (CFD) techniques. From a simple approach that models the gases leaving the bed toward the freeboard as a boundary condition [1–3] to detailed models that consider each existing particle in the packed bed [4,5], a wide range of model have been proposed. Two main types of strategies can be distinguished: the models that calculate the packed bed out of the CFD computational domain and the models that simulate the bed region. The first type of model is computationally efficient but limited to steady calculations with low accuracy in terms of the bed reactive processes. The second type is more accurate but usually expensive in terms of computational resources. As advances in calculation capabilities have allowed the computation of packed beds into the CFD domain to be made feasible, several proposals of this strategy have been shown in recent years. Two main modeling approaches, discrete element models (DEMs) and Eulerian beds, stand out as the most promising strategies to represent the thermal conversion of the bed. Several references are available for each type of approach. The DEM refers to the family of models that calculate the motion and interactions of a large number of small particles and the Eulerian is the approach that considers the bed of particles as a flow through field variables. On the one hand, the DEM-CFD combination shown in Refs. [6–9] shows a high accuracy in the tracking and thermal conversion of each particle, which gives a detailed representation of the reacting fronts inside the bed region. DEM-CFD implementation is widely used for the simulation of fluidized beds. Detailed particle tracks are needed to model the interaction between biomass and inert particles. Some examples of the multiple works that applied this technique can be found in Refs. [10,11]. Another common use of DEM-CFD is to simulate the combustion in furnaces in which the fuel is pulverized and affected

* Corresponding author.
E-mail addresses: miguelgr@uvigo.es (M.A. Gómez), cesalvarez@uvigo.es (C. Álvarez-Bermúdez), schapela@uvigo.es (S. Chapela), anca-couce@tugraz.at (A. Anca-Couce), porteiro@uvigo.es (J. Porteiro).

https://doi.org/10.1016/j.energy.2023.128243
Received 1 March 2023; Received in revised form 11 May 2023; Accepted 22 June 2023
Available online 29 June 2023

by strong gas streams [12] or to simulate cyclone-type particle separators [13]. It is also used for gas-solid fluidized bed analysis, however, as it requires a high computational effort, its application is limited to small-scale reactors. The DEM-CFD implementation has also been successfully applied to the simulation of biomass packed beds by a research group of Ruhr-Universität of Bochum. They tested the modeling technique capabilities and resolution of the reactive fronts inside the bed [4,14,15] and applied this method to assess the performance of different combustion systems [6,8,9]. On the other hand, the Eulerian approach considers the packed bed as a continuous porous zone in which each cell represents the average properties of the particles in that region. The Eulerian approach cannot be considered to be accurate as DEM modeling at the particle scale, but the Eulerian approach has been proven to work properly at the bed scale [16–19]. The main advantage of this approach is that it is computationally competitive in large-scale systems and thus has been previously applied in the simulation of 4 MW boilers [20,21] or even to fluidized beds [22].

An important aspect in biomass combustion modeling is the particle thermal treatment regarding the internal gradients of temperature. On the one hand, the simpler particle approach is the "thermally thin" (T. Thin) treatment, which considers a uniform particle temperature. This has an acceptable behavior for small particles (powder) or particles with a Biot number lower than 0.1. On the other hand, the "thermally thick" (T. Thick) treatment considers the internal temperature gradients, and it is important to take into account the reaction fronts on a particle scale. The Biot dimensionless number yields the ratio of the heat transfer resistance inside the particles to the heat transfer resistance on the surface of the particles. The thermally thick approach is recommended when the particle Biot number is higher than 0.1. In addition to the thermal gradients, the composition gradients are important to consider the intra-particle reactiveness accurately; in the case of biomass, composition gradients arise from the thermal gradients due to the temperature dependence of the decomposition reactions. The need to consider the internal reactive fronts in the biomass particles is indicated by a Thiele modulus higher than 1 [23] since the Thiele modulus compares the reactiveness and the diffusion of the combustion in a packed bed. The T. Thick approach is computationally expensive, which is an important limitation in regard to simulating beds with large amounts of particles. A complete review on combustion of thermally thick fuels and the whole set of CFD models involved was presented by Haberle et al. [24]. Several authors have studied several thermally thick particle models at particle scales [25–30]. The work from Gómez et al. [29] and, more recently, Chen et al. [30] can be highlighted in which a new combustion model for thermally thick biomass particles is proposed, which considers intra-particle heat conduction, radiation, reactions, and internal/external flow interactions. From the last paper can be extracted that oxygen mass fraction has an important impact on combustion behavior, and different pyrolysis characteristics and flame structures are observed in the combustion of square and rectangular particles. However, the application of T. Thick to the bed scale is more limited. Some examples of research that applied T. Thick treatment to large beds are [31–35]. Despite these works on both model types, there is a lack of studies on the comparison of both approaches and their performance and convenience to apply to study cases. Ku et al. [34] proposed a thermally thick particle model that is combined with the Euler-Lagrange model to study the biomass pyrolysis process in a fluidized bed reactor. They demonstrated that smaller particle size and higher temperature promote the pyrolysis process and reduce the time period during which the core temperature approaches the surface temperature. Wang et al. [35] integrated a model that couples a reactive computational fluid dynamic-discrete element model (CFD-DEM) with a one-dimensional thermally thick model to simulate biomass pyrolysis in a rotary drum. The effects of the rotation speed on several parameters were studied and it was found that a higher rotating speed or filling level has a negative impact on biomass conversion. Recently, Deng et al. [36] introduced the multiple thermally thick particle model for fixed-bed co-combustion using low-quality solid residues. The model was validated using wood and potato as representative fuels and showed satisfactory agreement with experimental results. They observed asynchronous conversion, particularly for high-moisture fuels, where the drying process extends across the entire conversion zone and overlaps with devolatilization. The limitation of these works is the highly time-consuming models only allow to simulate 2D or 3D small reactors for a few seconds.

Few studies assessed the behavior of both particle approaches and stated the ranges of acceptance. Remacha et al. [37,38] analyzed the effect of intra-particle gradients in devolatilization of biomass particles in the diameter range 3–15 mm under high temperatures and heating rates. They found that the T. thick model fit the data for all conditions and particle sizes, while the T. thin model failed to fit the trends observed in the data. Neglecting internal gradients leads to a delayed onset and abrupt release of volatiles. Otherwise, Gómez et al. [32] found that, despite the differences of behavior in a particle scale, in a packed bed both models predict similar ignition front rates and overall temperatures when the packed bed reacts with low oxygen conditions, but not for over-stoichiometric air conditions.

A DEM model is extremely computationally expensive to track a large number of particles at each time step. The Eulerian model, on the other hand, is not as computationally expensive and can work with longer time steps, although it does not achieve such precise resolution in the motion and location of the particles. As the reactor simulated in the present paper can be considered relatively large, since it holds more than 20,000 particles or even much larger quantities when the combustion is advanced and the bed accumulates particles of a reduced size, this work implements both thin and thick particle treatments in Eulerian CFD simulations via a comprehensive model. Several updates in the thermochemical conversion of the bed combined with improvements on the bed movement submodels, heat and mass transfers, and gas phase interactions are applied. The modeling with the two particle treatments is tested through several simulations of the combustor in which the bed and gas temperatures and the released volatiles are measured at several positions at the pyrolysis region to assess the models with a wide variety of parameters.

2. Model description

2.1. Assumptions

General assumptions.

- The porous medium is treated as a disperse medium with local averaged properties within each computational cell
- Within each cell, all particles are identical and represented by a characteristic particle.
- The particles in the bed are assumed to be spherical-equivalent
- Drying occurs at a specific temperature and is thermally controlled
- A three-step mechanism, commonly used in biomass combustion models, is used to model the devolatilization of dry wood
- Convection and radiation are used for gas-solid heat exchange, while conduction and radiation are used for solid heat exchange.
- The gases released by the solids are introduced into the gas phase at the same temperature as the solid phase
- Gases are assumed to be perfect
- The particle's degradation does not result in the formation of fissures or fragments.
- The ash content of the particle is non-reactive

Thermally thin model assumptions.

- There is a unique temperature in the whole particle
- The product gases generated inside the particles are immediately released into the gas phase, resulting in an immediate outflow condition

Thermally thick model assumptions.

- The particles are modeled as spheres with concentric internal layers, with no preferential directions
- Material properties are constant within each layer
- Char heterogeneous reactions occur at the outer layer of the particle, resulting in a shrinking core regime
- The released gases exchange heat with the external layers of the particle

2.2. Thermally thin approach

When a Eulerian CFD approach is applied to a biomass packed bed of particles, the bed is considered a porous medium in which both particles and gas are dispersed inside the volume of the computational cells. This means that all the gas and solid mass properties are locally constant in a cell. In addition, the thermally thin approach is based on the assumption of a constant temperature for the whole particle. The main consequence of this lack of thermal gradient inside the particle is that the decomposition proceeds uniformly throughout the particle volume. This is more accurate to represent the physical behavior when modeling particles with a lower Biot number. Fig. 1 shows a schematic of the thermally thin approach applied to a cell in a Eulerian packed bed.

The solid is characterized by several properties with conservation equations that define the evolution of the particles and, consequently, the packed bed. The conservation equations (Equation (1) to (7)) that represent the evolution of the biomass properties are listed in Table 1. Therefore, the combustion stages are related by the temperature and the change in the densities of the biomass components. We have adopted this method over the last decade in several works [18,21,39–41] that simulated different combustion systems such as boilers, burners or grates with complex geometries, since this method is especially efficient in beds with many particles.

This model is implemented in a CFD environment in which several submodels are needed to calculate the reaction rates that appear in the conservation equations and the interaction of the solid and gas phases. This involves a set of submodels, described in depth in Ref. [18], that solve the heat and mass transfer between the solid and gas phases.

2.3. Thermally thick approach

A more accurate model at the particle scale is an approach that considers the internal thermal and composition gradients of the particles. However, a refined discretization of the particles can lead to an extremely high computational effort. To address this, Thunman et al. [42] proposed a model that considers a particle layer for each of the biomass components, and consequently, the layer interfaces represent

Table 1
Conservation equations for the solid phase [41].

Solid phase enthalpy	$\frac{\partial(\varepsilon\rho_{part}h_s)}{\partial t} = \nabla(k_{s,eff}\cdot\nabla T_s) + S_{h_s}$	(1)
Solid fraction	$\frac{\partial \varepsilon}{\partial t} = \left(\frac{-\dot{\omega}'''_{wood}}{\rho^s_{wood}} + \frac{\dot{\omega}'''_{G,char} - \dot{\omega}'''_{c,char}}{\rho^s_{char}}\right)\varepsilon$	(2)
Particle diameter	$\frac{\partial d^3_{eq}}{\partial t} = \left(\frac{-\dot{\omega}'''_{wood}}{\rho^s_{wood}} + \frac{\dot{\omega}'''_{G,char} - \dot{\omega}'''_{c,char}}{\rho^s_{char}}\right) d^3_{eq}$	(3)
Moisture density	$\frac{\partial(\varepsilon\rho_{moist})}{\partial t} = -\dot{\omega}'''_{moist}\,\varepsilon$	(4)
Dry wood density	$\frac{\partial(\varepsilon\rho_{wood})}{\partial t} = -\dot{\omega}'''_{wood}\,\varepsilon$	(5)
Char density	$\frac{\partial(\varepsilon\rho_{char})}{\partial t} = (\dot{\omega}'''_{G,char} - \dot{\omega}'''_{c,char})\varepsilon$	(6)
Ash density	$\frac{\partial(\varepsilon\rho_{ash})}{\partial t} = 0$	(7)

the combustion fronts inside each particle. In this way, the particle can be discretized with only a few elements that are representative to model the biomass components and combustion stages with a feasible computational cost. This approach was applied by some authors [5,28] on a particle scale. The authors of this work also applied this approach with an efficient algorithm that allows us to apply the model in a large bed of particles [32]. This model is now improved so that it can be applied in beds with complex geometries and can represent the complex movements produced in the grates.

In the present model, the particles are discretized into four layers that represent the moist wood, dry wood, char, and ash present in the biomass. The variables of this particle model are the volumes and the temperatures of the four layers. The temperatures represent the average temperature of each layer and are considered uniform, which affects the reaction and consumption rates of the layers. The edges of the layers, which represent the reaction fronts, move toward the centers of the particles as the combustion advances. Therefore, combustion begins with a particle of moist wood, and the rest of the layers are created on the external surface and grow when their internal layer is consumed. Fig. 2 shows a schematic of the particle discretization and the subgrid scale inside the particle. These variables are calculated through finite volume techniques applied to the subgrid, following the notation shown in Fig. 3 for each element (P). The temperatures of the layers are described with the conduction equation for a spherical geometry, and then spatial and temporal discretization is applied (Equation (1)). This equation can be linearized as a function of the temperatures of the different layers, and when it is applied to the four layers, the result is a system of linear equations that can be algebraically solved (Equation system (2)). The details of this statement can be found in the paper presented by Gómez et al. [32]. The volumes of the layers are solved

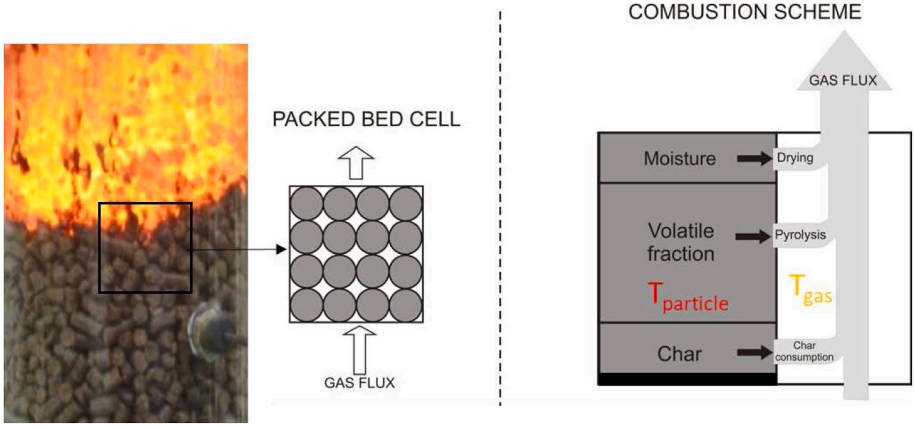

Fig. 1. Scheme of the thermally thin approach.

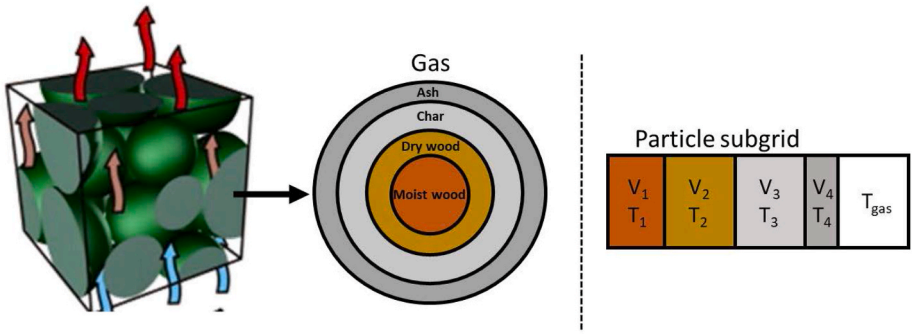

Fig. 2. Schematic of the thermally thick approach.

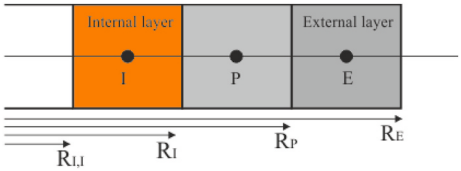

Fig. 3. Representation of the finite element notation in the subgrid-scale approach.

$$\frac{(\rho Cp)_P T_P - (\rho Cp)_P T_P^0}{\Delta t} V_P = 8\pi k_{P,E} \cdot R_E^2 \frac{T_E - T_P}{R_E^2 - R_I^2} - 8\pi k_{I,P} \cdot R_I^2 \frac{T_P - T_I}{R_P^2 - R_{I,I}^2} + S_{h,P} V_P \quad (1)$$

$$\begin{pmatrix} a_{P,1} & -a_{E,1} & 0 & 0 \\ -a_{I,2} & a_{P,2} & -a_{E,2} & 0 \\ 0 & -a_{I,3} & a_{P,3} & -a_{E,3} \\ 0 & 0 & -a_{I,4} & a_{P,4} \end{pmatrix} * \begin{pmatrix} T_1 \\ T_2 \\ T_3 \\ T_4 \end{pmatrix} = \begin{pmatrix} a_{P,1}^0 T_1^0 + b_1 \\ a_{P,2}^0 T_2^0 + b_2 \\ a_{P,3}^0 T_3^0 + b_3 \\ a_{P,4}^0 T_4^0 + b_4 \end{pmatrix} \quad (2)$$

$$\frac{V_P - V_P^0}{\Delta t} = S_{V_P} \quad (3)$$

$$\begin{pmatrix} a_{P,1} & 0 & 0 & 0 \\ -a_{I,2} & a_{P,2} & 0 & 0 \\ 0 & -a_{I,3} & a_{P,3} & 0 \\ 0 & 0 & -a_{I,4} & a_{P,4} \end{pmatrix} * \begin{pmatrix} V_1 \\ V_2 \\ V_3 \\ V_4 \end{pmatrix} = \begin{pmatrix} a_{P,1}^0 V_1^0 \\ a_{P,2}^0 V_2^0 \\ a_{P,3}^0 V_3^0 \\ a_{P,4}^0 V_4^0 \end{pmatrix} \quad (4)$$

with a similar algorithm that starts with volume conservation (Eq. (3)), which is a linear equation that can be applied to the four layers to obtain another system of linear equations (4). The novelties of the model used in this work regarding the model applied in Ref. [32] are the consideration of the ash layer in the volume subgrid and the elimination of the advective source term. The latter novelty is achieved because there is no advective movement of the bed during the CFD calculations. The bed movements occur at the end of the time steps following the algorithms presented in Ref. [43]. Although the particles are modeled like spheres, properties such as equivalent diameter and sphericity are considered in the functions related to the volume and surface of a particle so that these functions can be adapted to other types of particles. This is important in the interaction between solid and gas phases since it affects the fuel reactivity and the heat exchange with gas.

To quantify the range of application of the T. Thick model, the more general heat transfer approach is that, as previously mentioned, it is recommended when the Biot number is higher than 0.1, which, for biomass particles means a diameter (or characteristic length) greater than a value that can vary from 0.5 to 1.5 mm, depending on the air velocity. Even though there is no much research to determine the application range accurately for biomass combustion applications, we can outstand the works published by Remacha et al. [37,38]. They demonstrated the need the T. thick model for spherical particles biomass particles with a diameter greater than 3 mm.

2.4. *Bed and gas phase* ***modeling***

2.4.1. *Bed reaction and physics*

Both particle approaches are implemented for a packed bed that can occupy the computational volumes defined as porous zones, and the interaction between the solid and gas phases in these regions is modeled through volumetric sources. For the consumption rates, both models apply the same pyrolysis and char consumption kinetics. Pyrolysis is modeled through the Ranzi-Anca-Couce (RAC) scheme, the details of which are shown in Refs. [44,45]. This scheme is based on the proportions of lignin hemicellulose and cellulose to calculate the volatile gas fractions produced during devolatilization. The tars are lumped in a representative species, and the char has a fixed composition of $CH_\alpha O_\beta$, with $\alpha = 0.3934$ and $\beta = 0.0484$. Both the pyrolysis and char reaction kinetics are summarized in Table 2.

Char consumption considers oxidation and gasification reaction rates. The diffusion of oxygen, CO_2 and H_2O although the gas phase is also considered to control the consumption. The CO/CO_2 ratio produced in char oxidation proposed by Pedersen [46] is applied.

In the simulation of any combustion system where multi-particle fuels are used, it is important to represent the movements of the particles inside the packed bed. To address this, we have developed several submodels that represent the movements produced by the feeding systems and the crumbling and compaction produced by gravity when the particles shrink and lose their mechanical strength due to chemical degradation. These models are explained in detail in previous works [18, 43], and the comparison with an experimental method shows reasonably good results, especially considering that the movements of individual particles are modeled in a Eulerian approach that considers the bed as a continuous mass with averaged properties of the particles in the cells. Both submodels are based on the change in the solid phase variables that represent the mass and energy movements across the cell faces. The crumbling submodel moves the mass in the gravity direction and allows limited lateral movements while the bed piles do not exceed an angle of repose. The fuel feeding submodel produces bed movements from a fuel inlet following a certain direction. This is based on filling the cells with the fuel and discharging the excess mass in the feeding direction until no cells overflow.

The main inter-particle interaction, which is produced by the heat transfer between particles, is modeled through the packed bed diffusivity and the radiative exchange. The diffusivity is modeled through the bed effective thermal conductivity coefficient ($k_{s,eff}$) in Equation (1) for the T. Thin model. For the T. Thick model, the term $\nabla(k_{s,eff} \cdot \nabla T_s)$ is introduced through a source term in the external layer. The radiative

Table 2
Species and kinetics of the RAC scheme.

Pyrolysis	Kinetic [1/s]	Enthalpy of reaction [MJ/kg]	Refs.
$Dry\ wood \rightarrow 0.2336\ Char(CH_\alpha O_\beta) + 0.0821\ CO + 0.1141\ H_2O + 0.1243\ CO_2 + 0.0057\ H_2 + 0.0165\ CH_4 + 0.0131\ C_2H_4 + 0.4106\ Tar$	$K^{pyr} = 2e^{08} \cdot exp\left(-133100/_{R \cdot T_S}\right)$	0.0	[44, 47]
Char reactions	**Kinetics [m/s]**	**Enthalpy of reaction [MJ/kg]**	**Refs.**
$Char(CH_\alpha O_\beta) + (1 - \eta/2 + \alpha/4 - \beta/2)O_2 \rightarrow \eta CO + (1-\eta)CO_2 + \alpha/2 H_2O$	$K^{ox} = 5.7e^{07} \cdot exp\left(-160400/_{R \cdot T_S}\right)$	$-8.39 \cdot \eta - 29.88 \cdot (1-\eta)$	[48]
$Char(CH_\alpha O_\beta) + CO_2 \rightarrow 2CO + (\alpha/4)H_2 + \beta H_2O$	$K^{g.1} = 3.42 \cdot T_S \cdot exp\left(-15600/_{T_S}\right)$	15.876	[42, 49]
$Char(CH_\alpha O_\beta) + (1-\beta)H_2O \rightarrow CO + (1 + \alpha/2 - \beta)H_2$	$K^{g.2} = 5.7114 \cdot T_S \cdot exp\left(-15600/_{T_S}\right)$	12.693	[49]

exchange is calculated equally for both models. The radiative transfer equation (RTE) calculates the radiation exchange between the solid and gas phases of the cell and the surroundings for all directions of the modified DO model, as detailed in Ref. [50]. Another inter-particle interaction is the mechanical friction produced in the bed movements. In this work, the friction between particles is included in the angle of repose of the piles formed by the crumbling model, as detailed in Ref. [43].

2.4.1.1. Gas phase modeling. The gas phase is solved by using the classical CFD techniques and submodels commonly used in this type of work. The modeling is based on flow conservation equations such as continuity, momentum, turbulence, chemical species, and gas energy, which are efficiently solved by CFD codes.

Turbulence is solved through the realizable k-ε model. The reaction of species and its interaction with turbulence is modeled by finite-rate/eddy-dissipation due to its easy convergence in transient simulations. As radiation plays a key role in combustion applications, a modified discrete ordinate (DO) model [50] is used to take into account both solid and gas phases in the RTE and take advantage of the directional resolution of the classical DO model. In the bed zone, the porous media formulation is applied to take into account the section reduction and the particle interaction with the gas flow.

The gas mixture is modeled by the most common species, such as water vapor (H_2O), hydrogen (H_2), carbon dioxide (CO_2), carbon monoxide (CO), oxygen (O_2) and nitrogen (N_2), and representative hydrocarbons, such as methane (CH_4), ethylene (C_2H_4) and tars with an average molecule of $C_{2.35}H_{3.97}O_{1.53}$. Table 3 shows the reaction scheme applied to the gas phase and the reaction kinetics. All tar cracking reactions are grouped in a unique reaction in which Liden et al. [51] kinetics are applied.

2.4.1.2. Numerical methods and grid characteristics. The simulations in this work are successfully computed using first-order upwind schemes for the spatial discretization of the turbulence and second-order schemes for the rest of the variables. The pressure velocity coupling is solved through the SIMPLE scheme, and the gradients are calculated by a least squares cell-based algorithm. The transient formulation is solved with a first-order implicit method for all the variables.

The mesh basically involves the gas zones and the packed bed. Gas zones are the primary, secondary air injections and tertiary discuss plenum, combustion zones, and heat exchangers. In addition, the solid elements of the boiler are also meshed. The boundary conditions for the three combustion zones and heat exchanger that are cooled, convection to water, are considered. For the rest of the walls, still air convection is applied. In the internal walls, radiation is applied with an emissivity of 0.8 since the walls of the reactor are covered with a fouling layer. The air inlets are modeled as mass flow inlets with the flow rates listed in Table 4.

The geometry is discretized through a polyhedral mesh, which allows a reduction in the total number of elements with good quality that favors convergence, especially of the bed movements [43]. The grid is especially refined in the regions in which high gradients are produced, such as the air injections or the flame and the packed bed zones. Based on the experience of previous works [21,32,33,43] with similar models and simulations with different grid refinements, a one-million element mesh is used for all the simulations presented in the results section. The

Table 4
Boiler operating conditions.

Parameter	Unit	w8 WOR	w30 WOR	Error (%)
Fuel flux equivalent power	kW	32.7	28.7	
Fuel mass flow	kg/h	6.8	8.3	<1
$\lambda_{primary}$	–	0.20	0.21	
Primary air mass flow	kg/h	7.5	7.4	<3
Fixed bed height	m	0.25	0.25	<1
Primary air temperature	°C	20.0	22.7	<0.75

Table 3
Gas phase homogeneous reaction scheme.

Stoichiometry	Kinetics	Enthalpy of reaction [MJ/kg]	Refs.
$C_{2.35}H_{3.97}O_{1.53}(tar) \rightarrow 0.3\ C_2H_4 + 0.25\ CH_4 + 0.89 H_2 + 1.21\ CO + 0.16\ CO_2 + 0.13\ C(soot)$	$4.26e^{06}\ exp\left(-\frac{1.08e^{08}}{R \cdot T}\right)\left[C_{2.35}H_{3.97}O_{1.53}\right]$	−20.918	[45,51]
$C_2H_4 + 2\ O_2 \rightarrow 2\ CO + 2\ H_2O$	$1.35e^{10}\ exp\left(-\frac{1.2552e^{08}}{R \cdot T}\right)[C2H4]^{0.1}[O_2]^{1.65}$	−26.991	[52]
$CH_4 + O_2 \rightarrow CO + H_2 + H_2O$	$5.012e^{11}\ exp\left(-\frac{2e^{08}}{R \cdot T}\right)[CH4]^{0.7}[O_2]^{0.8}$	−17.296	[53,54]
$CO + 0.5\ O_2 \rightarrow CO_2$	$2.03e^{11}\ exp\left(-\frac{1.28e^{08}}{R \cdot T}\right)[CO][O_2]^{0.5}[H_2O]^{0.5}$	−10.103	[54]
$H_2 + 0.5\ O_2 \rightarrow H_2O$	$9.87e^{08}\ exp\left(-\frac{3.1e^{07}}{R \cdot T}\right)[H_2][O_2]$	−119.98	[55,56]

transient simulations are run up to a steady state. Five-second time steps are used, with 50 iterations per time step, which allow reasonably good convergence of each time step, especially as the steady state is approaching.

3. Experimental system

The models shown in the present paper are tested against the experimental data collected in a biomass reactor working with different fuels. A complete data collection system is installed in the reactor to analyze the temperatures and volatile composition at different points on the reaction region.

The experimental tests are carried out using a procedure in which the reactor is operated for continuous periods of up to 10 h. After the tests, the fuel feeding stops to finish the combustion and remove ash. All the data are collected when the system is working in a stationary state. These stationary conditions are determined when the air and fuel feeding mass flow rates are stable and the bed height is kept at 25 cm without any slagging. The measurements of all tests are repeated to ensure repeatability. The temperatures shown in the results section are the average measurements during the steady state measuring periods and the species through gas extractions in the measurement positions during periods of 12 min. More details on the experimental procedure are explained in Ref. [57].

3.1. Reactor

The experimental plant is a square-shaped reactor with a lateral fuel feeding inlet and bottom air supply designed to operate in low primary air conditions. The combustor walls are made of refractory bricks and a perforated grate in the bottom to allow air feeding. The plant is designed to work for up to 10 h in a row with an operating power of 30 kW. After the operation, the accumulated ash is removed across the bottom gate. The fuel feeding inlet is located 18 cm above the bottom. Fig. 4 shows a representation of the plant and the reactor zone. The fuel mass flow rate is regulated to keep the bed height constant through a position sensor, so the values given below in Table 4 show the average mass flow rates measured during the experiments when the steady state is reached.

A grid of measuring points is implemented in the reactor consisting of four measuring planes at different heights with nine thermocouples per plane and nine gas extractions at the highest plane. Fig. 5 shows the locations of the thermocouples and the gas extractions. The measuring planes are located at 5, 11, 17 and 32 cm over the bed bottom. More details of this data collection system are shown in Ref. [57].

Two different tests, in which fuels with different moisture contents are simulated in this work. The water content in the tests is 8% (w8 WOR) and 30% (w30 WOR). The operating conditions of the boiler are regulated to operate with a similar air flow rate in a quasi-steady mode. The measured operating conditions of the boiler for these two tests are shown in Table 4.

3.2. Fuel

The fuels used in the experiments were wood chips with different water contents. The average sphericity of these chips is estimated to be 0.4, and the equivalent spherical diameter is 10 mm. The bed packing is estimated to be 0.41, and the particle density is 467.4 kg/m^3 [57] resulting a fuel bulk density of 191.6 kg/m^3. The fuel composition, such as the moisture content, dry basis elementary analysis, ash fraction and heating values of the fuel used in both (w8 and w30) experiments, are shown in Table 5. The accuracy on the fuel proximate and elementary analysis is in the range 0.1–0.2%. However, the heterogeneity of the fuel samples, even when taken from the same batch of fuel, has an uncertainty of about 1%. The same occur with the heating values. The tests error is in the order of 0.3%, much lower than the error produced by the fuel heterogeneity.

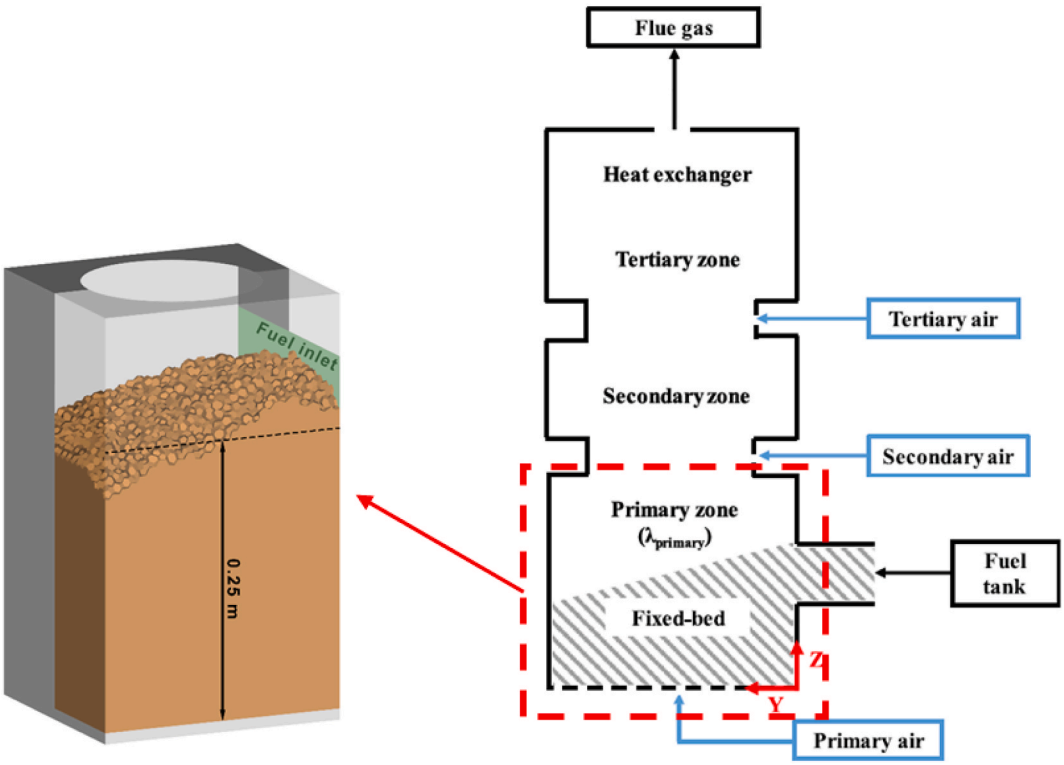

Fig. 4. Representation of the experimental reactor. Adapted from Ref. [57].

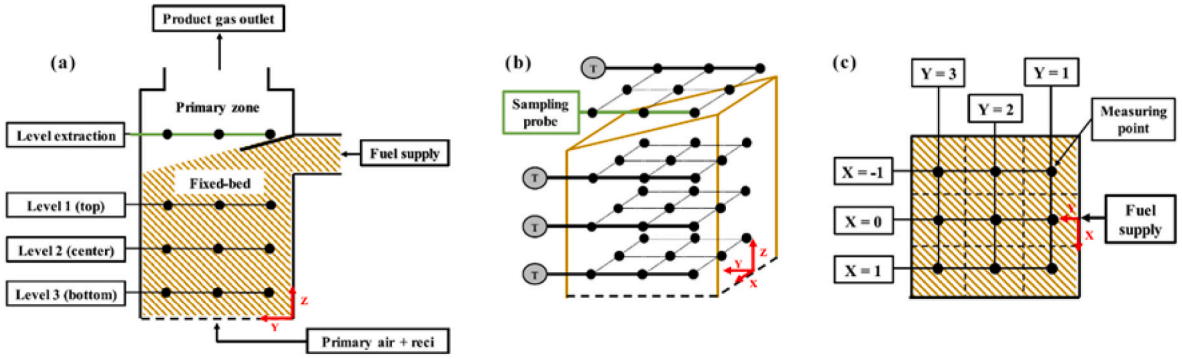

Fig. 5. Scheme of the data collection system. (a) Vertical view, (b) oblique view, (c) top view. Adapted from Ref. [57].

Table 5
Fuel properties and elementary analysis.

Parameter	Unit	Wood chips (w8)	Wood chips (w30)
Moisture content	[%][a]	8.0	30.7
C content	[%][b]	50.7	50.7
H content	[%][b]	6.0	6.0
O content	[%][b]	42.5	42.5
N content	[%][b]	0.1	0.1
Ash	[%][b]	0.7	0.7
GHV	MJ/kg[b]	20.4	20.4
NHV	MJ/kg[a]	17.4	12.4

[a] Wet basis, as received.
[b] Dry basis with ash. GHV: Gross heating value. NHV: Net heating value.

4. Results and discussion

In this section, we analyze the results of the simulation of the experimental tests (w8 WOR and w30 WOR) with both thermally thin (T. Thin) and thermally thick (T. Thick) approaches in a global Eulerian model. In the analysis, a comparison between model behavior and the comparison with an experimental contrast is performed. The parameters used in the assessment are mainly the temperature distribution in the bed and the main volatile species released over the bed (gas extraction zone).

The simulations start with the bed volume filled with fuel, which is ignited by applying an energy source in the whole bed volume for 2 min. This energy source produces a high amount of char and a high temperature in the whole bed, which stabilizes the combustion when the fuel feeding starts. Then, the simulation is run until the steady state is reached. The data shown in this section and the comparisons with the experimental tests correspond to steady-state conditions.

The calculations for this work were performed through 8-core CPU of 4.5 GHz. If a case is initialized from scratch, it can take two weeks to reach the steady state. Nevertheless, most cases were calculated from a "hot" case by changing the boundary conditions or fuel properties. These cases can converge to the steady state in approximately five days, depending on the abrupt of the change of conditions.

4.1. Temperature distribution

The temperature distributions predicted by the models can be seen in Fig. 6 (T. Thin) and Fig. 7 (T. Thick). As a general result common to both models, the bed top is colder than the bed bottom. On the one hand, the fresh fuel is fed from a side of the bed top and advances to the bottom as it is consumed. On the other hand, the primary air is introduced through the bed bottom, and the char is consumed in this region, which produces a high temperature. In addition, the volatiles are consumed in the secondary air region, which is out of the bed, and their reactions do not have a significant effect on the bed temperature profile. Therefore, the bed temperature decreases with the bed height. The first clear difference

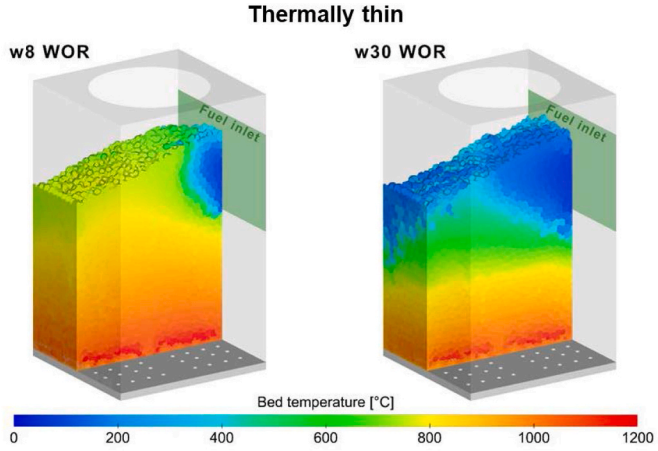

Fig. 6. Packed bed temperature for the tests (w8 WOR and w30 WOR) predicted by the thermally thin model.

is that the T. Thick model can consider four different temperatures while the T. Thin can consider only an average temperature, which is inherent to the models. This gives the T. Thick model a higher accuracy in the definition of reaction fronts, since it allows an overlapping of the conversion stages. The same particle can be dried in the inner layer at 100 °C, and the dry wood and char layers can react at 600 °C, as illustrated in the bed top in Fig. 7. This is not possible with the T. Thin model, since the temperature hardly rises over 100 °C during drying in this case, while devolatilization is virtually zero under 300 °C. In the T. Thick model, the moist wood and dry wood temperatures are not shown in the lower region of the bed since these layers are completely consumed at this region. The external layers exist in the whole bed because their temperature is the one used in the heat exchange with the surroundings, even in the virgin particles in which this layer exists with a non-significant volume. The temperature distribution of the T. Thin model is similar to the char and surface temperature distribution in the T. Thick. The decrease produced when rising from the bottom to the top is more aggressive in the T. Thick model, especially for the w8 WOR case.

The variation in the temperatures can be compared in Fig. 8. As experimental temperatures were measured at nine positions and four heights, this figure shows the average of the nine temperatures along the bed height for the simulations and the experimental averaged measurements at the four heights. The predicted temperatures consider the equilibrium temperature that a thermocouple would measure in each position. This takes into account the equilibrium between the radiation and convection in a spherical thermocouple [18]. It is an average between the gas temperature and the radiation temperature (affected mainly by the particle temperature in the cell but also in the neighboring cells). For both the T. Thin and T. Thick approaches, the temperature of

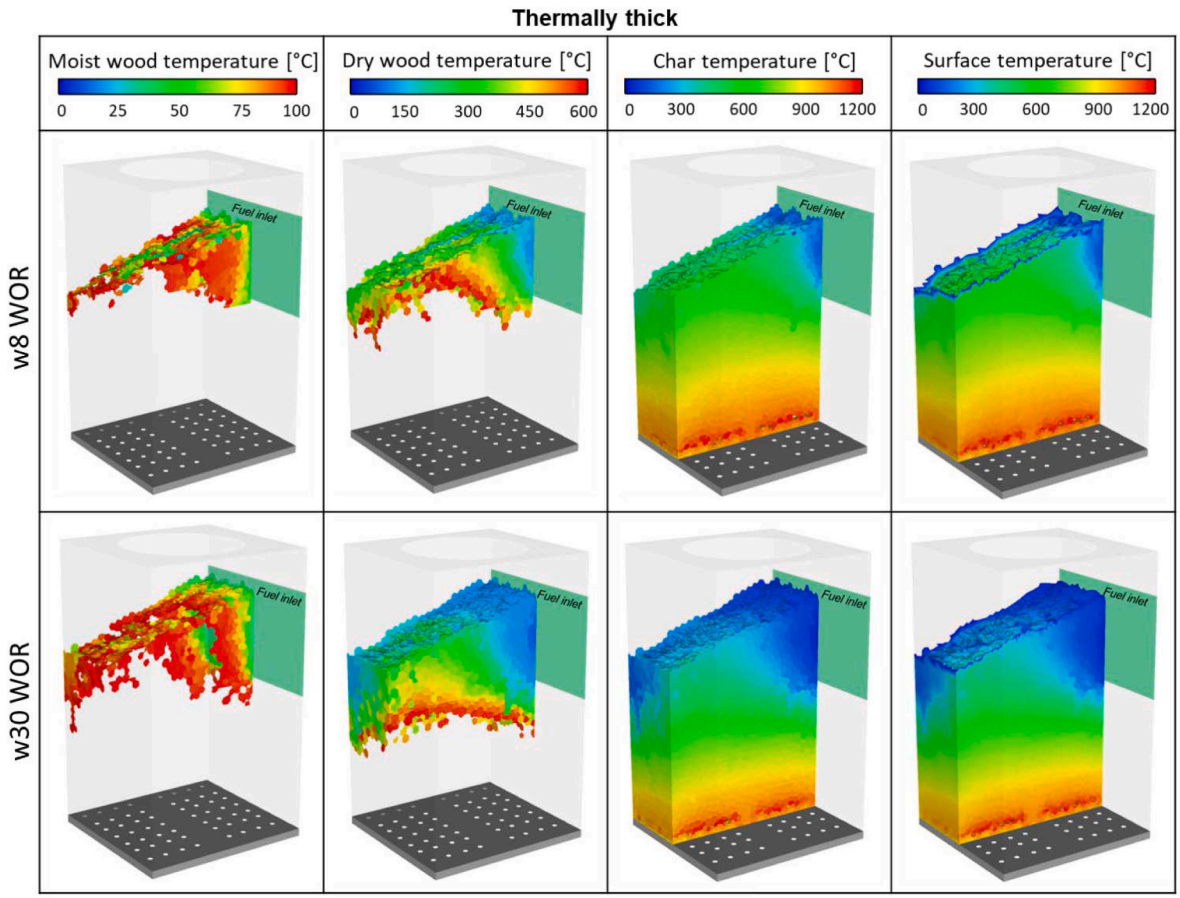

Fig. 7. Temperature of moist wood, dry wood, char and ash (surface) layers for the tests (w8 WOR and w30 WOR) predicted by the thermally thick model.

the thermocouples is calculated in the same way. Nevertheless, the radiation temperature of a particle is calculated from the surface temperature for the T. Thick model and from the average temperature for the T. Thin.

The comparison of the T. Thin and T. Thick models shows a faster decrease in the T. Thick model in the w8 WOR experiment. This may be because the external layer is thin and is easily cooled by the gas in the T. Thick model. Otherwise, in the T. Thin model, the temperature corresponds to the whole particle, which has a higher inertia and is not so strongly affected by the gas cooling. For the w30 WOR test, both models show a similar average temperature variation with height. It seems that the high moisture content equalizes the behavior of both models.

In the comparison with experimental measurements, both models show reasonably good predictions for all the bed heights except in the lower area of the bed in the w30 WOR experiment, in which the predicted temperatures are clearly lower than the measurements for both models, and the upper region of the bed for the T. Thin model, where the thermocouple temperature is overpredicted.

The conclusion drawn based on these results is that although the T. Thick model should be more accurate in terms of temperature prediction, it is not clear that either of the two models exhibits a better performance. This may be caused by the use of wood chips in the experimental tests, since wood chips are far from thermally thick spherical particles.

4.2. Reaction fronts

One of the advantages of these models is the accuracy in the visualization of the biomass component contours, which are a good indicator of the reaction fronts. The distributions of moisture, dry wood and char in the bed of the T. Thin model are shown in Fig. 9 for both cases, w8 WOR and w30 WOR. The influence of the moisture content has an important effect on the reaction fronts and the distribution of all densities. In the w8 WOR case, the moisture and dry wood densities are only present in the region close to the fuel inlet, which means that drying and pyrolysis take place entirely in that region, and the rest of the bed is occupied by the char, except the bottom, where ash is located. In the w30 WOR simulation, the high moisture content delays the drying and pyrolysis processes. Therefore, the moisture and, especially, the dry wood reach the rear wall. This means that the drying and pyrolysis front are distributed along the whole bed surface.

The distribution of the particle layers and the reaction fronts of the T. Thick model are shown in Fig. 10. In this case, the moisture content also has some influence but does not drastically change the bed distributions, as with the T. Thin model. Moist wood and dry wood are present not only close to the fuel inlet in the w8 WOR case but also along the bed surface. Char is present in deeper layers of the bed, and ash is only present in the bed bottom. In the w30 WOR case, the presence of moist wood and dry wood is also distributed from the fuel inlet to the rear wall but in a higher area in comparison with the w8 WOR case. The moist wood and the dry wood spread over the entire surface, but the dry wood reached deeper layers of the bed. The char and the ash occupy similar regions as in the T. Thin simulation. The results of both models show very similar bed heights for both experimental cases, which is a good result of the simulation method since the experimental boiler was regulated to work with a constant bed height. Therefore, as the fuel mass flow rate and, especially, the fuel flux equivalent power of both experiments are clearly different but the air mass flux is almost the same, this shows that the moisture content affects the bed height.

These distributions of the biomass components and reaction fronts are important to explain the volatile species distributions shown below.

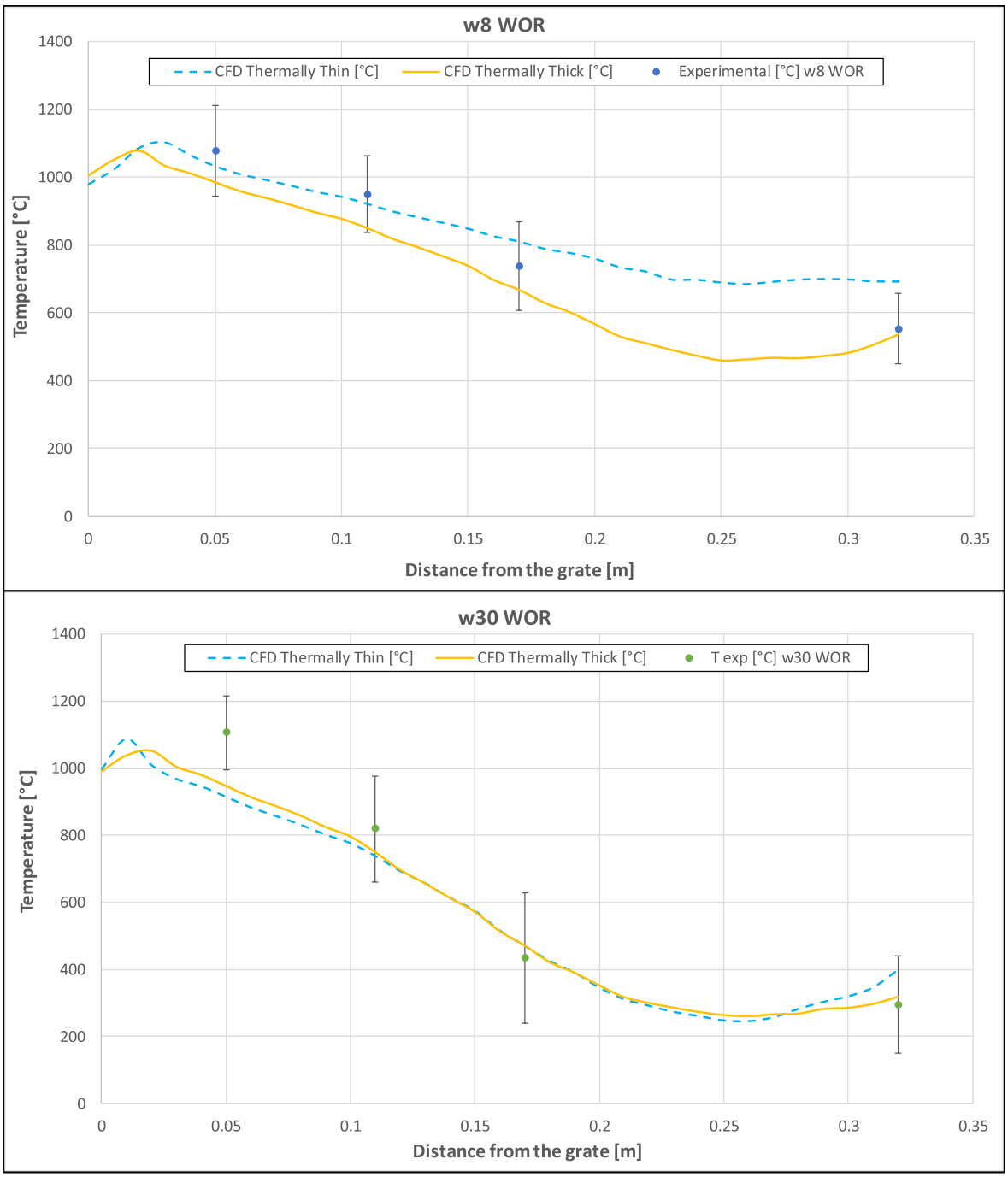

Fig. 8. Temperature (average of the nine positions shown in Fig. 5 (c)) variation with height from the bed bottom. Data taken from CFD simulations and experiments.

4.3. Volatile distribution

As previously stated, the volatile composition was tested in the experimental plant through gas extraction at nine positions over the bed (shown in Fig. 5) at a height of 32 cm over the bed bottom. The same positions are assessed in the simulations performed with the models. The measurements of the volatile species concentrations are tar free and dry. In this section, the volume fractions of the predominant species (except N_2), CO, CO_2 and CH_4, and the mass concentration of tar are shown for both model predictions and experimental measurements.

Figs. 11–14 present the results of the spatial distributions of the concentrations of CO, CO_2, CH_4 and tar on the gas extraction plane, just over the bed surface. The results of both models, thermally thin and thermally thick, are shown in comparison with the measurements.

As a general view, both models predict the volatile concentrations with reasonably similar values considering the relative simplicity of the models in comparison to the complex phenomena occurring in biomass combustion processes. The maximum error considering the averaged values on the measuring plane is lower than 35%. Fig. 11 shows relatively similar values of CO concentration for both models, but the trends are different from the experimental results. The T. Thin and T. Thick models show similar trends for the w30 WOR case but different trends for the w8 WOR case. Fig. 12, which compares the CO_2 fractions of both models, also shows similar behavior of the models in the case of the w30 WOR, with good predictions. In the case of the w8 WOR, whereas the T. Thick model has a more homogeneous CO_2 distribution, the T. Thin releases more CO_2 near the fuel supply. This is caused by the temperature distribution. As seen in Fig. 6, the devolatilization front,

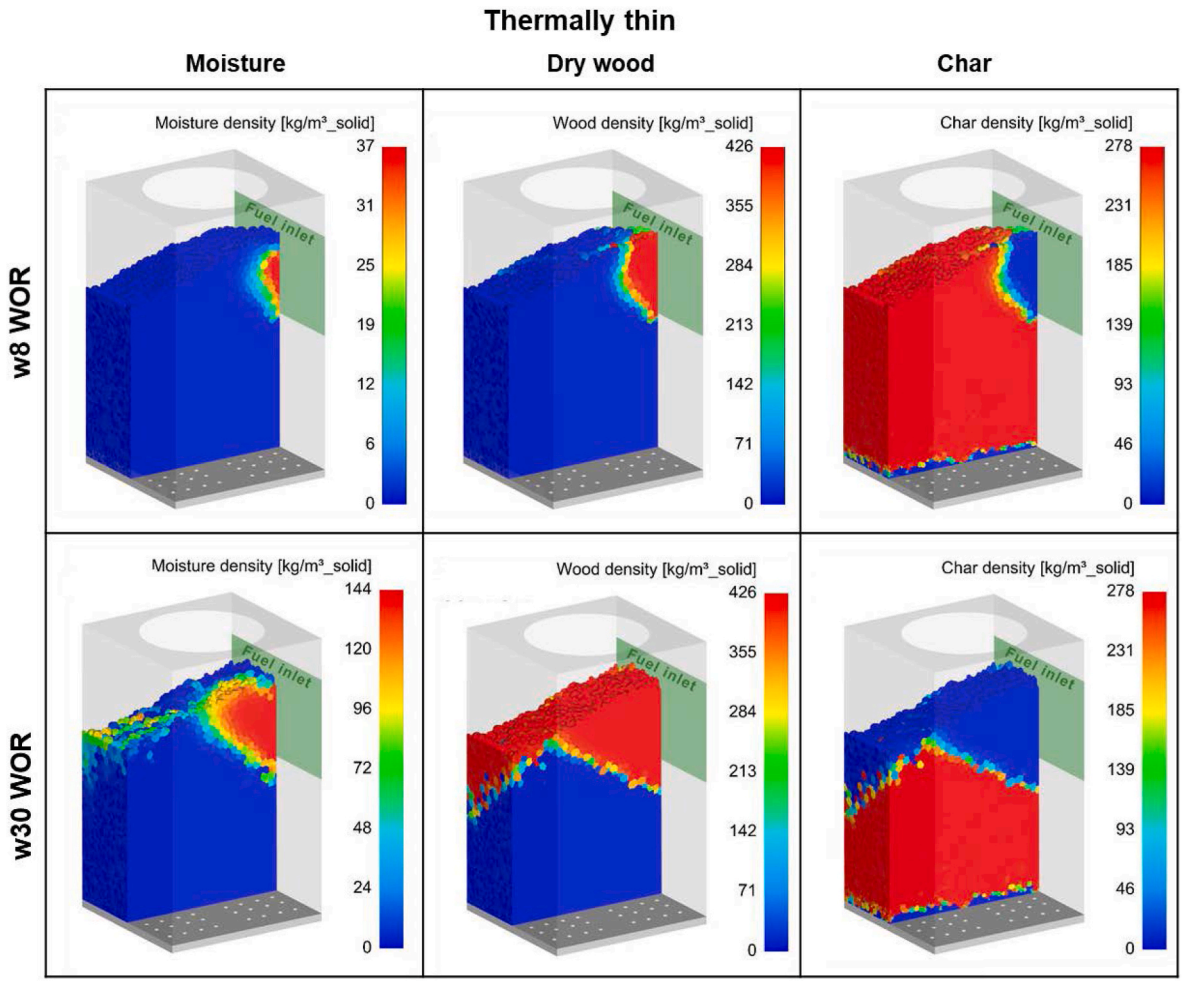

Fig. 9. Contours of the densities of moisture, dry wood and char in the thermally thin model.

corresponding to a temperature range of 300–600 °C, is located close to the fuel inlet. However, the T. Thick model presents a devolatilization front that spreads to the highest region of the bed (Fig. 7). In the experimental comparison, both models again present relatively accurate predictions in global terms. The CH_4 distribution results are presented in Fig. 13. Again, both models present similar trends and accurate predictions in the w30 WOR case. However, they present some differences in the w8 WOR case. As with the CO_2 profiles, the T. Thick model has a more homogeneous distribution, and the T. Thin presents higher concentrations in the surroundings of the fuel inlet. It can also be explained by the differences in the distribution of the devolatilization fronts for both models. Finally, Fig. 14 shows the distribution of tar concentrations. For this species, again, the models behave similarly in the w30 WOR simulations, but although the values are in the same range, the experimental trends are not captured. In the w8 WOR case, the T. Thin model nearly captures the experimental values for most positions, which does not happen with the T. Thick model.

The average of the measurements and model predictions at the nine extraction positions can be used to reflect the success of the models. Fig. 15 compares the average values of the model predictions and experimental measurements for the volume fractions of CO, CO_2 and CH_4 and the mass concentration of tar. Both models give similar averaged values, which can be expected since both models use the same devolatilization, char conversion and chemical reactions, but the temperature distributions are different, which affect the conversion rates. The predictions are reasonably accurate for the analyzed species considering the complexity of the processes and the amount of species and reactions involved in the bed thermal conversion. The average errors of the T. Thin and T. Thick models are 8% and 12%, respectively. The maximum deviation found is 34% error in the prediction of CO_2 for the T. Thick model.

Again, both models present a similar behavior based on the experimental comparison of volatile compositions. A slightly more accurate behavior may be observed with the T. Thin model. This indicates that the T. Thin model may be more appropriate for the simulation of wood chips due to the "thin" geometry of this type of particle.

The T. Thick model gives a better prediction of the temperatures measured above the bed but a worse prediction of the volatiles distribution for the experiment (w8 WOR). It is important to note that the temperatures at the lowest heights (within the bed) are better predicted by the T. Thin model and the volatile measurements at that height are a consequence of the gases released in the lower bed. Therefore, it is consistent that the T. Thin model has a better prediction of the volatile concentrations at positions above the bed. On the other hand, for the experiment with a high-moisture fuel (w30) both models have a very similar behavior for both temperatures and volatiles.

5. Conclusions

Two different particle combustion approaches are implemented in a Eulerian biomass combustion model to simulate complete boilers. The first particle approach considers the particles as a thermally thin mass with the densities of the biomass components dispersed and mixed. The second particle approach considers thermally thick mass with four layers that can represent the biomass components and reaction fronts. Both particle models are applied to the simulation of an experimental

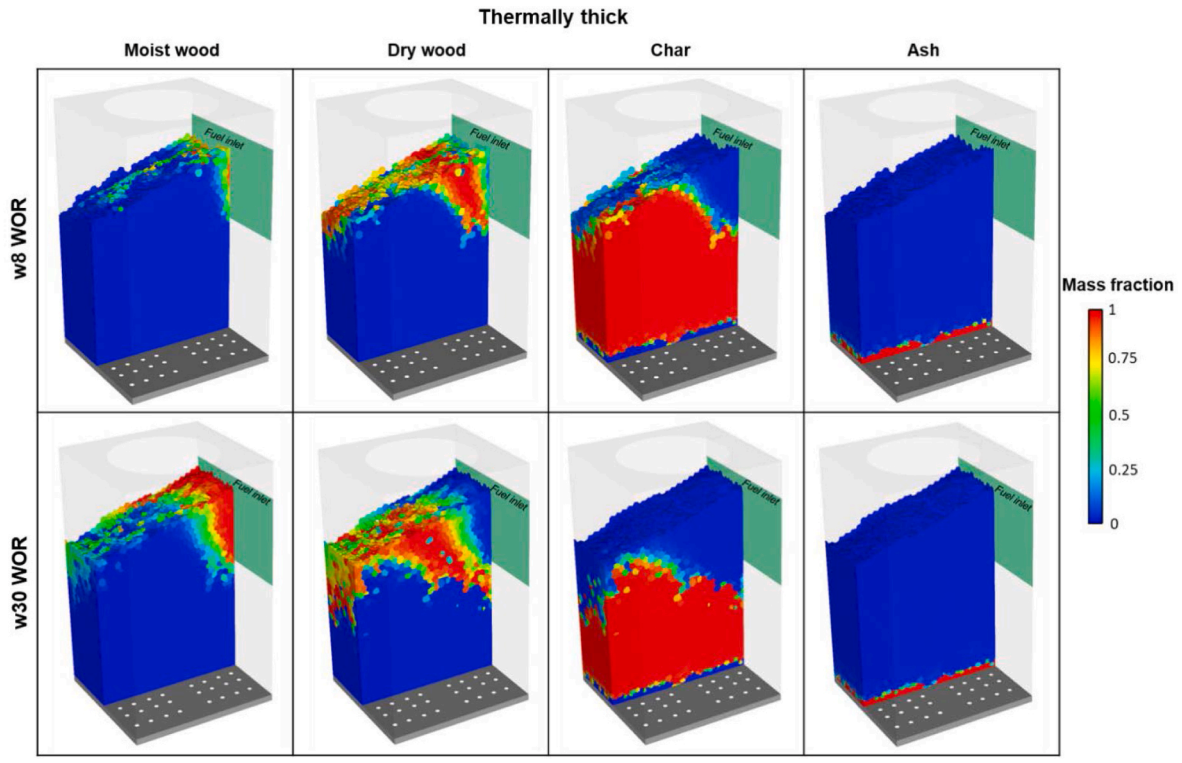

Fig. 10. Contours of the particle components (mass fractions of moist wood, dry wood, char and ash) in the thermally thick model.

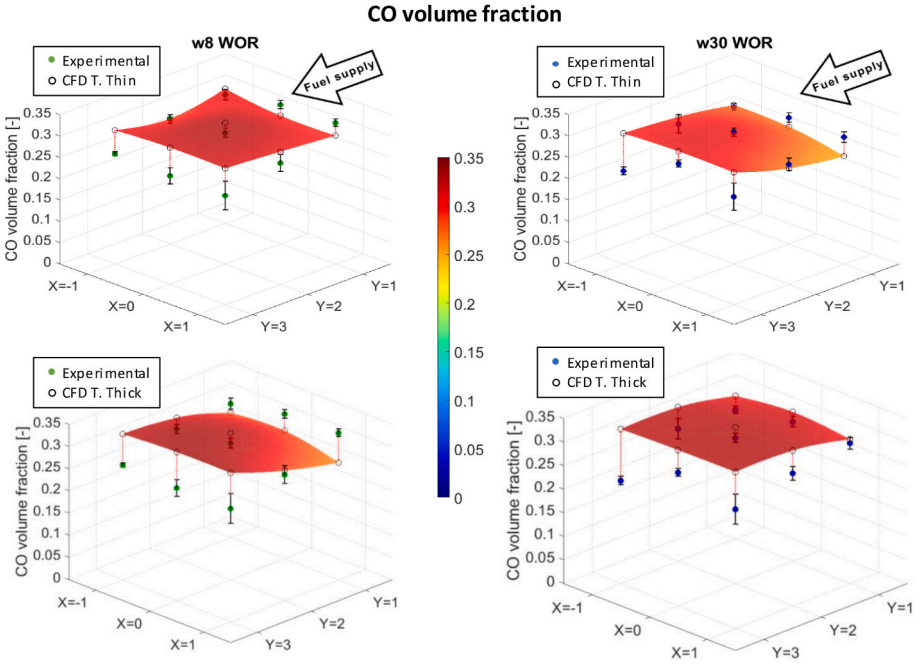

Fig. 11. Comparison of the experimental and predicted CO concentrations.

biomass boiler with a large packed bed in which the temperatures of several positions and the volatiles emitted by the bed are registered. Two experimental tests are simulated, in which fuels with 8% and 30% water content (w8 WOR and w30 WOR, respectively) are considered. The temperatures were registered at nine positions on each of four planes at different heights over the packed bed bottom.

The results show that both models produce similar thermocouple temperatures along the bed height for the w30 WOR case, but the T. Thick model produces a more abrupt temperature decrease in the higher bed layers. The comparison with the experimental measurements shows that the models follow a similar trend with reasonably similar values with the exception of the lowest plane in the w30 WOR case, in which models predict clearly lower temperatures, and the highest plane for the T. Thin model in the w8 WOR case, which overpredicts the temperature over the bed. With the predictions of the volatile concentrations in the plane located over the bed, the trends of both models are also compared

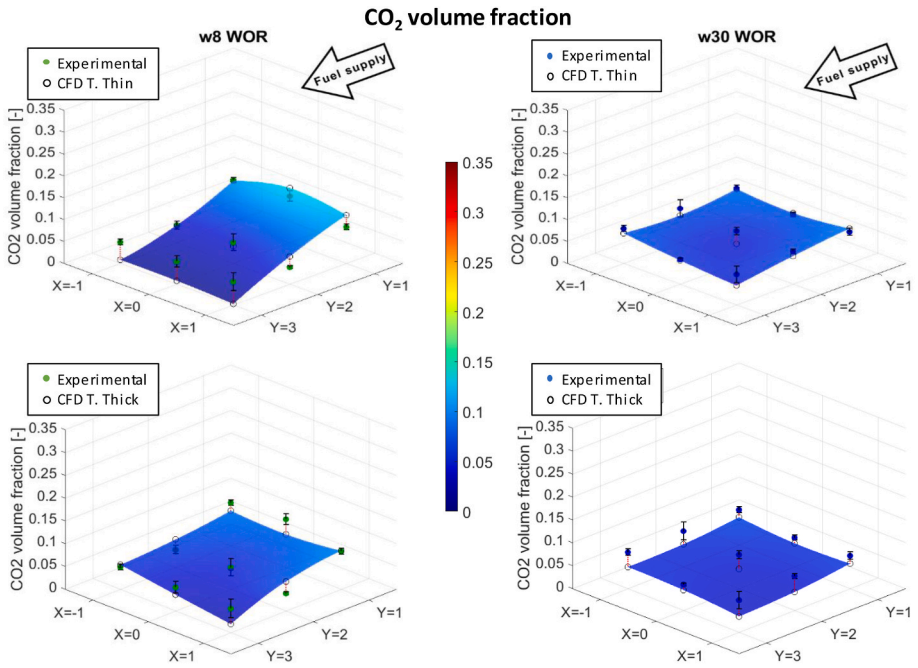

Fig. 12. Comparison of the experimental and predicted CO_2 concentrations.

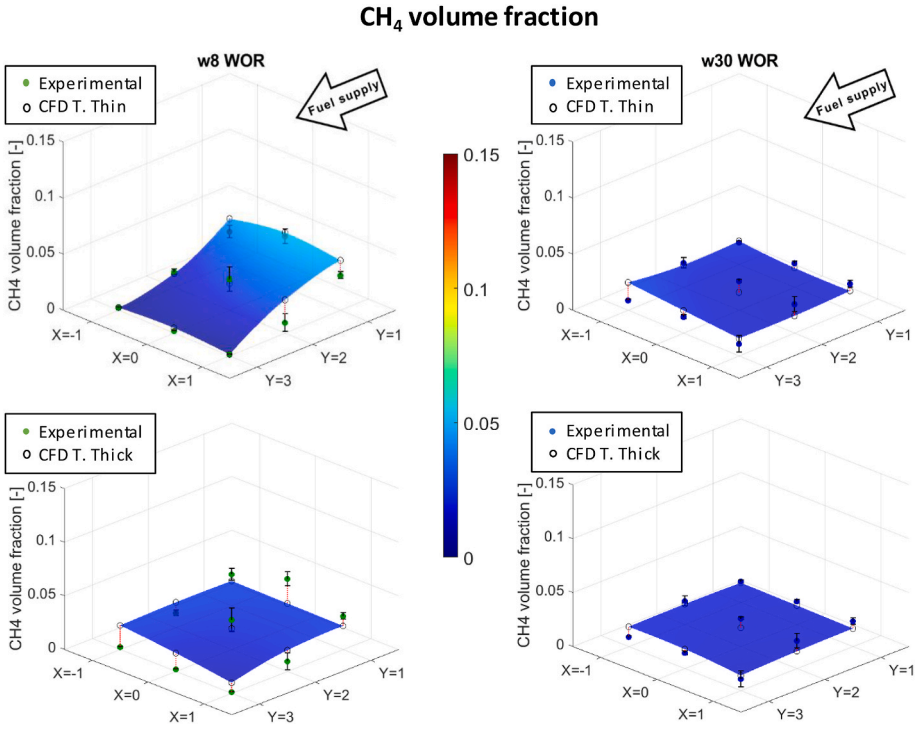

Fig. 13. Comparison of the experimental and predicted CH_4 concentrations.

and contrasted with measurements. Concentrations of CO, CO_2, CH_4 and tar are analyzed at the nine points of the plane. Both models predict a relatively homogenous profile in the plane with values reasonably close to the experimental measurements for the w30 WOR case. For the w8 WOR case, whereas the T. Thin model predicts higher concentrations of CO_2, CH_4 and tar in the region close to the fuel inlet, the T. Thick model predicts a more homogeneous distribution. The average values of the nine positions registered show that both models predict the volatile concentration in reasonably good agreement with the experiments, considering the complex processes involved in biomass thermal conversion. The average errors of the T. Thin and T. Thick models are 8% and 12%, respectively, for the measured species.

The overall comparison of both models with experimental results shows a similar behavior between the two models or a slightly better behavior for the T. Thin model. This indicates that for the simulation of wood chips, T. Thin may be more appropriate due to its slightly more accurate predictions and lower computational cost.

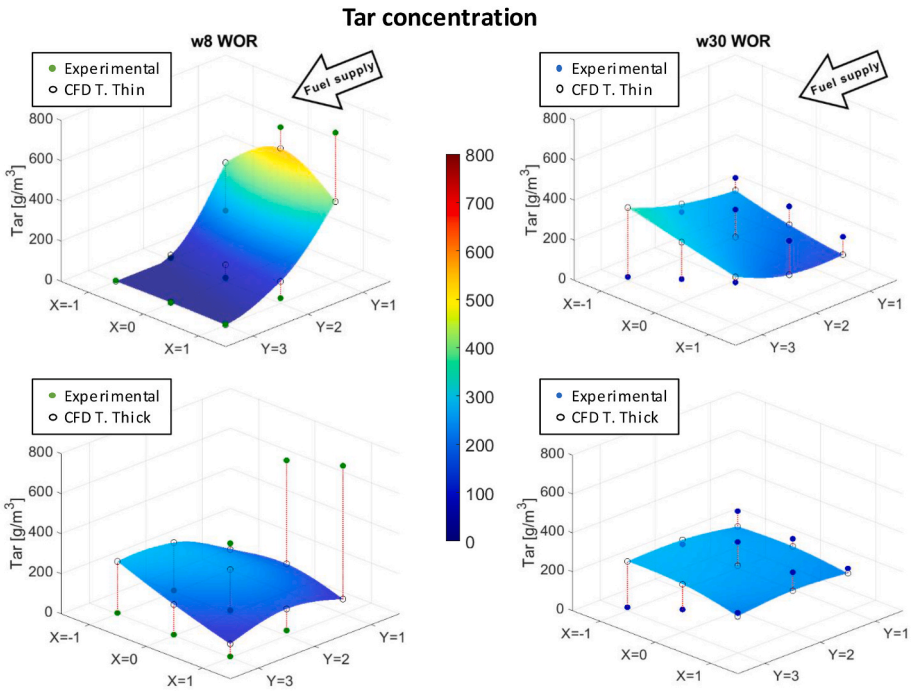

Fig. 14. Comparison of the experimental and predicted tar concentrations.

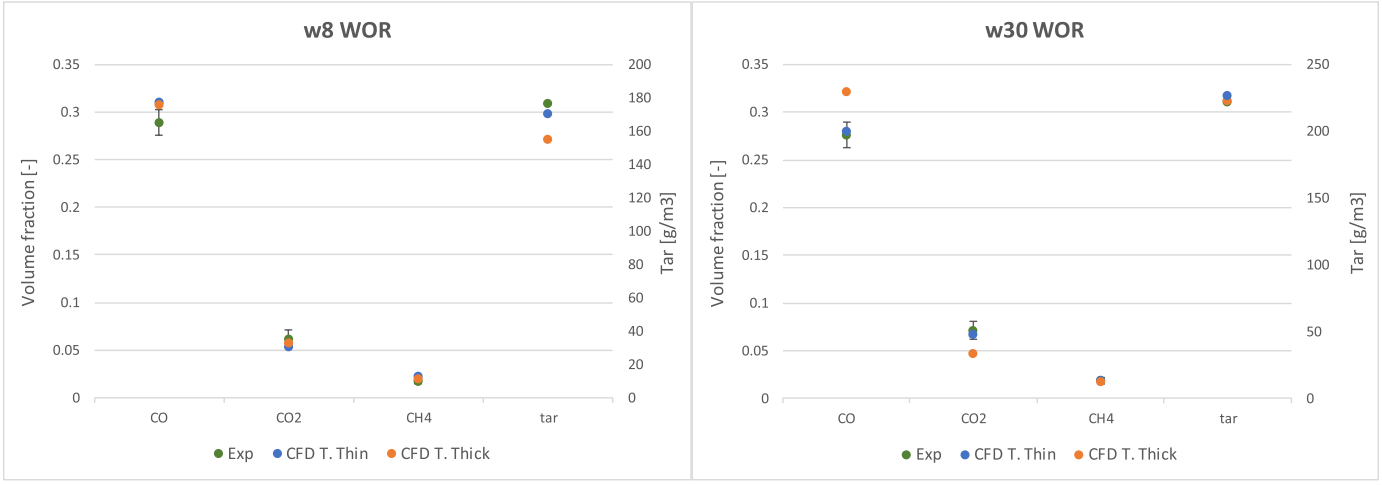

Fig. 15. Averaged volatile concentrations of models predictions and experimental measurements.

CRediT authorship contribution statement

M.A. Gómez: Conceptualization, Methodology, Investigation, Writing – original draft, Writing – review & editing, Supervision. **C. Álvarez-Bermúdez:** Conceptualization, Methodology, Investigation, Writing – original draft, Writing – review & editing. **S. Chapela:** Methodology, Investigation, Resources, Supervision. **A. Anca-Couce:** Methodology, Investigation, Visualization, Writing – review & editing, Supervision. **J. Porteiro:** Visualization, Resources, Supervision.

Declaration of competing interest

The authors declare that they have no known competing financial interests or personal relationships that could have appeared to influence the work reported in this paper.

Data availability

Data will be made available on request.

Acknowledgments

This research was financially supported by the project PID2021-126569OB-I00 of the Ministry of Science, Innovation and Universities (Spain). Funding for open access charge: Universidade de Vigo/CISUG.

Nomenclature

a	Linear equation coefficient ($W{\cdot}K^{-1}$ in the energy equation, s^{-1} in the volume equation)
b	Linear equation independent coefficient (W in the energy equation, $m^3{\cdot}s^{-1}$ in the volume equation)
Cp	Specific heat ($J{\cdot}kg^{-1}{\cdot}K^{-1}$)
d_{eq}	Equivalent spherical diameter (m)
h_s	Solid phase enthalpy ($J{\cdot}kg^{-1}$)
k	Thermal conductivity ($W{\cdot}m^{-1}{\cdot}K^{-1}$)
K	Char reaction constants ($m{\cdot}s^{-1}{\cdot}K^{-1}$)
R	Ideal gas constant ($J{\cdot}\ K^{-1}{\cdot}mol^{-1}$)
S	Source term ($W{\cdot}m^{-3}$)
T	Temperature (K)
t	Time (s)
V	Volume (m^3)

Greek

$\boldsymbol{\varepsilon}$	Solid fraction (−)
$\boldsymbol{\rho}$	Density ($kg{\cdot}m^{-3}$)
$\boldsymbol{\eta}$	Char oxidation parameter (−)
$\dot{\omega}_i^{'''}$	Generation or consumption rates of the wood components ($kg{\cdot}m^{-3}{\cdot}s^{-1}$)

Subscripts

ash	Ash content
c	Consumption
char	Char
E	External layer (thermally thick model)
eff	Effective
G	Generation
h	Enthalpy
I	Internal layer (thermally thick model)
I,I	Interior of the internal layer (thermally thick model)
moist	Moisture
P	Current layer (thermally thick model)
part	Particle
s	Solid
V	Volume
wood	Dry wood

Superscripts

0	Previous time step
g,1	Gasification reaction with CO_2
g,2	Gasification reaction with H_2O
ox	Char oxidation
s	Specific

References

[1] Kær SK. Straw combustion on slow-moving grates – a comparison of model predictions with experimental data. Biomass Bioenergy 2005;28:307–20.
[2] Van Der Lans RP, Pedersen LT, Jensen A, Glarborg P, Dam-Johansen K. Modelling and experiments of straw combustion in a grate furnace. Biomass Bioenergy 2000;19:199–208.
[3] Shin D, Choi S. The combustion of simulated waste particles in a fixed bed. Combust Flame 2000;121:167–80.
[4] Wiese J, Wissing F, Höhner D, Wirtz S, Scherer V, Ley U, Behr HM. DEM/CFD modeling of the fuel conversion in a pellet stove. Fuel Process Technol 2016;152:223–39.
[5] Mehrabian R, Zahirovic S, Scharler R, Obernberger I, Kleditzsch S, Wirtz S, Scherer V, Lu H, Baxter LL. A CFD model for thermal conversion of thermally thick biomass particles. Fuel Process Technol 2012;95:96–108.
[6] Buss F, Wirtz S, Scherer V. Combustion of straw pellets in an agitated fuel bed: experiments and DEM/CFD simulations. Combust Sci Technol 2022;194:195–212.
[7] Scherer V, Mönnigmann M, Berner MO, Sudbrock F. Coupled DEM–CFD simulation of drying wood chips in a rotary drum – baffle design and model reduction. Fuel 2016;184:896–904.
[8] Buss F, Wirtz S, Scherer V. Simulation of a reacting agitated bed of straw pellets by a resolved coupled DEM/CFD method using a blocked-off approach. Int J Therm Sci 2020:152.
[9] Wissing F, Wirtz S, Scherer V. Simulating municipal solid waste incineration with a DEM/CFD method – influences of waste properties, grate and furnace design. Fuel 2017;206:638–56.
[10] Wang S, Shen Y. Particle-scale study of heat and mass transfer in a bubbling fluidised bed. Chem Eng Sci 2021:240.
[11] Wu W, Duan L, Li L, Liu D. Investigation on a single char particle movement behavior in a bubbling fluidized bed under high temperature. Fuel Process Technol 2022:236.
[12] Wang S, Shen Y. CFD-DEM modelling of raceway dynamics and coke combustion in an ironmaking blast furnace. Fuel 2021:302.
[13] El-Emam MA, Zhou L, Shi WD, Han C. True shape modeling of bio-particulate matter flow in an aero-cyclone separator using CFD–DEM simulation. Comp Particle Mechanics 2021;8:955–71.
[14] Krause B, Liedmann B, Wiese J, Wirtz S, Scherer V. Coupled three dimensional DEM-CFD simulation of a lime shaft kiln-Calcination, particle movement and gas phase flow field. Chem Eng Sci 2015;134:834–49.
[15] Scherer V, Wirtz S, Krause B, Wissing F. Simulation of reacting moving granular material in furnaces and boilers an overview on the capabilities of the discrete element method. Energy Proc 2017;120:41–61.
[16] Khodaei H, Gonzalez L, Chapela S, Porteiro J, Nikrityuk P, Olson C. CFD-based coupled multiphase modeling of biochar production using a large-scale pyrolysis plant. Energy 2021:217.
[17] Karim MR, Naser J. Numerical study of the ignition front propagation of different pelletised biomass in a packed bed furnace. Appl Therm Eng 2018;128:772–84.
[18] Gómez MA, Porteiro J, Patiño D, Míguez JL. CFD modelling of thermal conversion and packed bed compaction in biomass combustion. Fuel 2014;117:716–32.
[19] Karim MR, Naser J. Progress in numerical modelling of packed bed biomass combustion. 2014.

[20] Karim MR, Naser J. CFD modelling of combustion and associated emission of wet woody biomass in a 4 MW moving grate boiler. Fuel 2018;222:656–74.
[21] Álvarez-Bermúdez C, Chapela S, Varela LG, Gómez MÁ. CFD simulation of an internally cooled biomass fixed-bed combustion plant. Resources 2021;10.
[22] Diba MF, Karim MR, Naser J. Fluidized bed CFD using simplified solid-phase coupling. Powder Technol 2020;375:161–73.
[23] Peters B. Classification of combustion regimes in a packed bed of particles based on the relevant time and length scales. Combust Flame 1999;116:297–301.
[24] Haberle I, Ø Skreiberg, Łazar J, Haugen NEL. Numerical models for thermochemical degradation of thermally thick woody biomass, and their application in domestic wood heating appliances and grate furnaces. Prog Energy Combust Sci 2017;63:204–52.
[25] Babu BV, Chaurasia AS. Heat transfer and kinetics in the pyrolysis of shrinking biomass particle. Chem Eng Sci 2004;59:1999–2012.
[26] Lu H, Robert W, Peirce G, Ripa B, Baxter LL. Comprehensive study of biomass particle combustion. Energy Fuel 2008;22:2826–39.
[27] Porteiro J, Granada E, Collazo J, Patiño D, Morán JC. A model for the combustion of large particles of densified wood. Energy Fuel 2007;21:3151–9.
[28] Ström H, Thunman H. CFD simulations of biofuel bed conversion: a submodel for the drying and devolatilization of thermally thick wood particles. Combust Flame 2013;160:417–31.
[29] Gómez MA, Porteiro J, Chapela S, Míguez JL. An Eulerian model for the simulation of the thermal conversion of a single large biomass particle. Fuel 2018;220:671–81.
[30] Chen T, Ku X, Lin J, Jin H. Modelling the combustion of thermally thick biomass particles. Powder Technol 2019;353:110–24.
[31] Mehrabian R, Shiehnejadhesar A, Scharler R, Obernberger I. Multi-physics modelling of packed bed biomass combustion. Fuel 2014;122:164–78.
[32] Gómez MA, Porteiro J, Patiño D, Míguez JL. Fast-solving thermally thick model of biomass particles embedded in a CFD code for the simulation of fixed-bed burners. Energy Convers Manag 2015;105:30–44.
[33] Gómez MA, Porteiro J, De la Cuesta D, Patiño D, Míguez JL. Dynamic simulation of a biomass domestic boiler under thermally thick considerations. Energy Convers Manag 2017;140:260–72.
[34] Ku X, Shen F, Jin H, Lin J, Li H. Simulation of biomass pyrolysis in a fluidized bed reactor using thermally thick treatment. Ind Eng Chem Res 2019;58:1720–31.
[35] Wang J, Ku X, Yang S. Simulation of biomass pyrolysis in a rotary drum by coupling CFD-DEM with a one-dimensional thermally thick model. Energy Fuel 2022;36:3665–79.
[36] Deng R, Wang L, Zhang R, Luo Y. Numerical modeling of fixed-bed cocombustion processes through the multiple thermally thick particle model. ACS Omega 2022;7:39938–49.
[37] Remacha MP, Jiménez S, Ballester J. Devolatilization of millimeter-sized biomass particles at high temperatures and heating rates. Part 1: experimental methods and results. Fuel 2018;234:757–69.
[38] Remacha MP, Jiménez S, Ballester J. Devolatilization of millimeter-sized biomass particles at high temperatures and heating rates. Part 2: modeling and validation for thermally-thin and -thick regimes. Fuel 2018;234:707–22.
[39] Chapela S, Porteiro J, Garabatos M, Patiño D, Gómez MA, Míguez JL. CFD study of fouling phenomena in small-scale biomass boilers: experimental validation with two different boilers. Renew Energy 2019;140:552–62.
[40] Gómez MA, Porteiro J, Patiño D, Míguez JL. Eulerian CFD modelling for biomass combustion. Transient simulation of an underfeed pellet boiler. Energy Convers Manag 2015;101:666–80.
[41] Gómez MA, Porteiro J, de la Cuesta D, Patiño D, Míguez JL. Numerical simulation of the combustion process of a pellet-drop-feed boiler. Fuel 2016;184:987–99.
[42] Thunman H, Leckner B, Niklasson F, Johnsson F. Combustion of wood particles – a particle model for Eulerian calculations. Combust Flame 2002;129:30–46.
[43] Varela LG, Gómez MA, Garabatos M, Glez-Peña D, Porteiro J. Improving the bed movement physics of inclined grate biomass CFD simulations. Appl Therm Eng 2021:182.
[44] Anca-Couce A, Scharler R. Modelling heat of reaction in biomass pyrolysis with detailed reaction schemes. Fuel 2017;206:572–9.
[45] Anca-Couce A, Sommersacher P, Scharler R. Online experiments and modelling with a detailed reaction scheme of single particle biomass pyrolysis. J Anal Appl Pyrolysis 2017;127:411–25.
[46] Pedersen K. The product ratio of CO/CO_2 in the oxidation of biomass char. 2003.
[47] Thunman H, Niklasson F, Johnsson F, Leckner B. Composition of volatile gases and thermochemical properties of wood for modeling of fixed or fluidized beds. Energy Fuel 2001;15:1488–97.
[48] Di Blasi C. Modeling wood gasification in a countercurrent fixed-bed reactor. AIChE J 2004;50:2306–19.
[49] Bryden KM, Ragland KW. Numerical modeling of a deep, fixed bed combustor. Energy Fuel 1996;10:269–75.
[50] Gómez MA, Patiño D, Comesaña R, Porteiro J, Álvarez Feijoo MA, Míguez JL. CFD simulation of a solar radiation absorber. Int J Heat Mass Tran 2013;57:231–40.
[51] Liden AG, Berruti F, Scott DS. A kinetic model for the production of liquids from the flash pyrolysis of biomass. Chem Eng Commun 1988;65:207–21.
[52] Westbrook CK, Dryer FL. Prediction of laminar flame properties of methanol-air mixtures. Combust Flame 1980;37:171–92.
[53] Dryer FL, Glassman I. High-temperature oxidation of CO and CH4. Symp Int Combust 1973;14:987–1003.
[54] Scharler R, Gruber T, Ehrenhöfer A, Kelz J, Bardar RM, Bauer T, Hochenauer C, Anca-Couce A. Transient CFD simulation of wood log combustion in stoves. Renew Energy 2020;145:651–62.
[55] Hsu K, Jemcov A. Numerical investigations of detonation in premixed hydrogen-air mixture – assessment of simplified chemical mechanisms. Fluids 2000 Conf Exhibit 2000. In: Tech. Rep. AIAA-2000-2478. Denver: American Institute of Aeronautics and Astronautics; 2000.
[56] Varma AK, Chatwani AU, Bracco FV. Studies of premixed laminar hydrogen-air flames using elementary and global kinetics models. Combust Flame 1986;64:233–6.
[57] Archan G, Anca-Couce A, Gregorc J, Buchmayr M, Hochenauer C, Gruber J, Scharler R. Detailed experimental investigation of the spatially distributed gas release and bed temperatures in fixed-bed biomass combustion with low oxygen concentration. Biomass Bioenergy 2020:141.